Synthetic Metals 158 (2008) 775–781

Contents lists available at ScienceDirect

Synthetic Metals

journal homepage: www.elsevier.com/locate/synmet

Photoelectrical behavior of perylene derivative/π-conjugated polymer system

Klára Podhájecká [a,*], Pavel Matějíček [b], Jiří Vohlídal [b], Toshio Masuda [c], Jiří Pfleger [a]

[a] Institute of Macromolecular Chemistry, Academy of Sciences of the Czech Republic, Heyrovsky Sq. 2, CZ-162 06 Prague 6, Czech Republic
[b] Department of Physical and Macromolecular Chemistry, Faculty of Science, Charles University in Prague, Hlavova 2030, CZ-128 40 Prague 2, Czech Republic
[c] Department of Polymer Chemistry, Graduate School of Engineering, Kyoto University, Katsura Campus, Kyoto 6158510, Japan

ARTICLE INFO

Article history:
Received 27 December 2007
Received in revised form 25 April 2008
Accepted 13 May 2008
Available online 21 July 2008

Keywords:
Poly(diphenylacetylene)
Organic photovoltaics
Heterojunction

ABSTRACT

Organic photovoltaic (PV) cells composed of a perylene derivative, *N*,*N*′-di(pentan-3-yl)-perylene-3,4:9,10-bis(dicarboximide), PTCDI, acting as an acceptor and a π-conjugated polymer poly{1-phenyl-2-[4-(trimethylsilyl)phenyl]acetylene}, PDPA, acting as a donor of photogenerated free electrons are presented. Two types of starting double-layer samples were prepared: samples I composed of a spin-cast PDPA thin film bottom layer and a PTCDI upper layer deposited by the vacuum sublimation, and samples II composed of a spin-cast mixed PDPA/PTCDI layer and a vacuum-sublimation deposited PTCDI upper layer. The samples were treated with toluene vapors to induce changes in the morphology of heterojunctions due to recrystallization of PTCDI, which have been monitored by the optical absorption spectra and AFM images, and the influence of the morphology changes on photovoltaic characteristics of the samples has been studied. A short-time (2–5 min) toluene-vapor treatment positively influences the PV efficiency of system I due to a formation of larger PTCDI crystals, which improves the collection efficiency of the upper layer. However, a longer-time treatment of a system I results in a decrease in its PV efficiency owing to a significant decrease in the PDPA–PTCDI interfacial area accompanying further growth of PTCDI crystals, which lowers the photogeneration efficiency of the system. A combination of molecularly dissolved (in PDPA) and crystalline PTCDI in the system II has been proved to provide better PV efficiency due to a combination of improved free charge carrier photogeneration in the composite bottom layer and the collection efficiency of charge carriers of the upper layer.

1. Introduction

The architecture of organic PV devices based on a heterojunction formed on the boundaries between donor and acceptor phases stems from two basic types of organization of the active components. The concept of heterojunction was first introduced using bilayer structures [1] with donor and acceptor molecules in layers stacked together with a planar interface. The advantage of such structure is a spatially uninterrupted pathway for the photogenerated charge carriers to the respective electrodes [2] but it has a relatively small active interface area limiting the overall energy conversion efficiency [3]. Later, it was shown that the bulk heterojunction [4–6], where donors and acceptors are intimately mixed in a bulk of the device, gives better efficiency than the bilayer structures due to an increased interfacial area where the exciton dissociation can occur. A diffuse bilayer heterojunction device in which the advantages of both bilayer and bulk heterojunction architectures are combined, is conceptually in-between these two approaches.

For the bulk heterojunction devices it has been shown that the optimal nanoscale phase separation of donor and acceptor components in a bicontinuous (interpenetrating) network is critical for their performance [7,8]. The scale of the phase separation should correspond to the diffusion length of excitons (ca 10 nm for π-conjugated polymers) and, simultaneously, the transport of photogenerated free charge carriers to a proper electrode should be optimized. The best performance has been achieved with polymer/fullerene blends [9–12], the heterojunction morphology of which depends on conditions of the active layer preparation such as a solvent used, solution concentration, temperature and rate of solvent evaporation, etc. Moreover, the morphology of blends composed of poly(3-hexylthiophene) and fullerene derivatives is being modified by a post-processing treatment, such as thermal annealing, which improves the PV efficiency due to a better separation of phases. To obtain functional interface in the diffuse bilayer heterojunction devices, many different strategies can be employed such as lamination of thin polymer films upon pressure and increased temperature application [6], spin-coating of a top layer from the solvent swelling

* Corresponding author.
E-mail address: podhajec@imc.cas.cz (K. Podhájecká).

0379-6779/$ – see front matter © 2008 Elsevier B.V. All rights reserved.
doi:10.1016/j.synthmet.2008.05.006

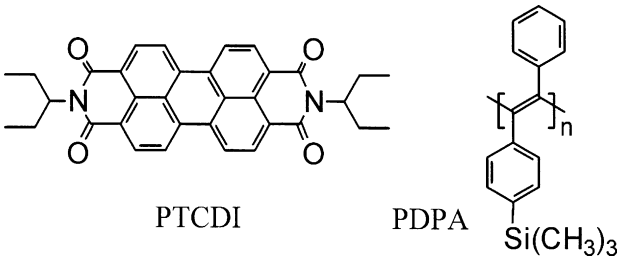

Fig. 1. Chemical structures of active components: poly{1-phenyl-2-[4-(trimethylsilyl)phenyl]acetylene} (PDPA) and *N*,*N*′-di(pent-3-yl)-perylene-3,4:9,10-bis (dicarboximide) (PTCDI).

the bottom layer [13] or by thermal annealing of a bilayer device [14].

Recently, we studied electronic properties of an oligomeric end-functionalized poly(diphenylacetylene) [15,16]. The introduction of benzoyl or fluorene-9,9-diyl end groups to poly(diphenylacetylene) molecules resulted in a substantial increase in the photogeneration efficiency for holes. However, the power conversion efficiency of PV cells prepared from these materials was too low owing to limitation of the optical absorption to the blue spectral region. Compared with polymers of monosubstituted acetylenes, which often undergo autoxidative degradation [17–21], poly(diphenylacetylene)s show excellent thermal and photochemical stability in air even in the UV spectral region [22–25]. Perylene diimides have been successfully applied to prepare photoconductive polymer composites of reasonable photovoltaic performance [26–29]. A property convenient for the use of these materials in PV devices is their ability to form crystals characterized by high exciton diffusion ranges in the order of micrometers [30,31] which is several orders of magnitude above the values usual for semiconducting polymers and other non-crystalline materials applied in the organic photovoltaics.

One possible way to improve the morphology of a polymer/low-MW compound blend is an exposure of the active layer to solvent vapor, the technique investigated namely in connection with reticulate doping [32,33]. In a previous article [34], we reported on morphological changes taking place during the solvent vapor treatment of the composite consisting of poly{1-phenyl-2-4-(trimethylsilyl)phenylacetylene} (PDPA), which acts as a donor upon photoexcitation, and a perylene derivative: *N*,*N*′-di(pent-3-yl)-perylene-3,4:9,10-bis(dicarboximide) (PTCDI) acting as an acceptor of photogenerated electrons (Fig. 1). We also found that the recrystallization of PTCDI occurring during the toluene-vapor treatment improves the PV efficiency of single layer devices based on these materials. In the present paper we report on double-layer devices composed of the same starting materials but possessing different architectures, one with bilayer heterojunction and another one with both bulk and bilayer heterojunctions, and on the effect of the solvent vapor treatment on their photovoltaic properties.

2. Experimental

2.1. Materials

N,*N*′-di(pent-3-yl)-perylene-3,4:9,10-bis(dicarboximide), PTCDI, was purchased from SynTec (Germany). PEDOT:PSS, poly[3,4-(ethylenedioxy)thiophene]:poly(styrenesulfonate) (Baytron P) was purchased from Bayer (Germany). Indium tin oxide-coated glass was purchased from Merck (Germany). π-Conjugated polymer: poly{1-phenyl-2-[4-(trimethylsilyl)phenyl]acetylene}, PDPA, was prepared by the polymerization of corresponding acetylene monomer induced with $TaCl_5$-based catalyst according to the procedure described earlier [22–25]. The polymer was yellow and its molecular-weight characteristics were determined using a size-exclusion chromatography device equipped with a multi-angle light scattering detector (MALS). Measurements were evaluated in two ways: (i) using the absolute method based on the MALS data: $M_n = 520 \times 10^3$; $M_w = 1035 \times 10^3$, and (ii) using the calibration curve method based on polystyrene (PS) standards: $M_n = 635 \times 10^3$; $M_w = 1690 \times 10^3$ (M_n and M_w are the number-average and weight-average polymer molecular weights, respectively). As can be seen, the absolute molecular weight values obtained using MALS data are somewhat lower than those obtained on the basis of PS standards, which proves an increased rigidity of double-substituted PDPA chains compared with that of PS chains.

2.2. Samples preparation

Two types of starting samples were prepared: (I) double-layer samples composed of PDPA layer (thickness 70 nm, prepared by the spin-casting from toluene) and an upper PTCDI layer (thickness 38 nm) deposited by the vacuum sublimation on the PDPA bottom layer and (II) double-layer samples composed of mixed PDPA/PTCDI layer (22 wt% of PTCDI, thickness 90 nm, prepared by the spin-casting from toluene) and an upper PTCDI layer (thickness 18 nm) deposited by the vacuum sublimation on the bottom layer. Indium tin oxide (ITO) glass coated with a PEDOT:PSS layer (thickness 30 nm, prepared by the spin-casting and dried in a vacuum at 110 °C for 1 h) was used as a substrate for both structures. The vapor-treatment of starting samples was done by exposing the samples to saturated toluene vapor at room temperature for various time periods. After a chosen exposition time, the sample was dried in a vacuum oven at 40 °C for 2 h to evaporate residual toluene. Samples for electrical measurements were finally coated with a top Al electrode prepared by the vacuum deposition technique.

2.3. Sample characterization

AFM measurements were performed using a scanning probe microscope NT-MDT NTEGRA Prima equipped with a Nanosensors silicon cantilever (typical spring constant 40 N m^{-1}); the tapping mode under ambient conditions was applied. UV/vis spectra of thin films cast on glass substrates were obtained using a spectrophotometer PerkinElmer Lambda 950. The spectra were not corrected for the reflected and scattered light, which explains the mutual shift of the baselines for individual absorption curves. Cyclic voltammograms of PDPA thin films drop-cast on a Pt electrode were obtained using a potentiostat AMEL Instruments 7050 (Italy), saturated calomel reference electrode and 0.1 M solution of tetrabutylammonium hexafluorophosphate in acetonitrile. The ferrocene/ferrocenium redox system was used as a standard, assuming that the HOMO level of ferrocene is 4.8 eV below the vacuum level. HOMO energy of PDPA (E_{HOMO}) was determined from the onset of oxidation peak ($E_{on} = 0.4$ V vs. ferrocene) as $E_{HOMO} = -(eE_{on} + 4.8)$. Photovoltaic measurements were made under steady-state conditions, using a xenon lamp (XBO 75) and a Jobin Yvon H25 monochromator as the light source, in a serial connection of the sample with a stabilized power supply Keithley 230 and an electrometer Keithley 617. The light intensity was measured in a reference beam derived by a beamsplitter using a calibrated photodiode EG&G HUV-1100B. The dark current was allowed to relax for 120 s for each wavelength as well as for each value of the voltage applied, and the photocurrent was recorded at a given time period after the optical shutter was opened. The photocurrent spectra are presented as a difference between currents measured under illumination and in the dark.

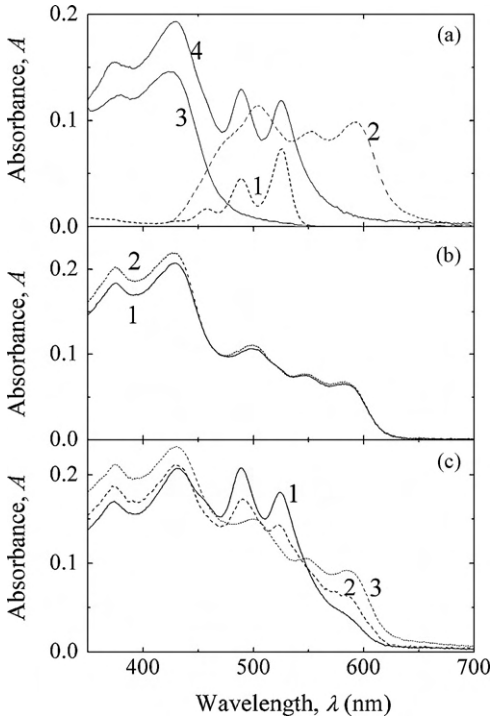

Fig. 2. Optical absorption spectra: (a) curve (1) PTCDI in toluene solution, (2) PTCDI thin film on a glass substrate after 18 h solvent vapor treatment, (3) PDPA thin film, and (4) film of untreated PDPA/PTCDI mixture (22 wt% of PTCDI, layer thickness 70 nm); (b) system I: curve (1) untreated, and (2) 15 min treatment with toluene vapor; (c) system II: curve (1) untreated, curve (2) 2 min treatment, curve (3) 15 min treatment.

3. Results and discussion

Optical absorption spectroscopy represents a convenient tool to follow the crystallization of PTCDI. In Fig. 2a, a spectrum of PTCDI in toluene solution (curve 1) and a spectrum of PTCDI deposited on a glass substrate are shown (curve 2). PTCDI in solution shows three distinct bands located at 525, 489 and 458 nm, which, according to the literature [35,36], can be ascribed to the vibronic progression of the S_0–S_1 transition in a single isolated PTCDI molecule.

Optical spectra of a PTCDI thin film deposited on a glass substrate and subjected to toluene vapor treatment do not show the bands characteristic of single PTCDI molecules but new, red shifted broad bands centered at 505, 554 and 594 nm (Fig. 2a, curve 2). These absorption bands should be attributed to transitions in PTCDI molecules packed in the crystal structure. Crystallization of discotic aromatic molecules is known to induce splitting of exciton energy levels giving rise to new bands in the absorption spectra [35,37]. Energies of these new states are given by the mutual orientation of transition dipole moments of chromophores aligned in the crystal lattice. If the dipoles are aligned linearly, so-called J-aggregates are formed and a bathochromic shift of the absorption band is observed in the absorption spectrum. If the molecular arrangement results in the coplanar orientation of transition dipoles of chromophores, so-called H-aggregates are formed and a hypsochromic shift occurs in the spectrum. Because molecular packing in real crystals is almost never ideally linear or coplanar, it mostly includes both these features displayed with various intensities depending on the incline angle of parallelly arranged transition dipoles; the critical angle being ca. 57°. Consistently, the new broad bands at 594 and 554 nm observed in our vapor-treated samples should be ascribed to PTCDI molecules packed in crystals as J-aggregates with incline angle above 57° (see similar results for other perylene carboxydiimides [35,37]). The band around 505 nm and the shoulder around 470 nm in solvent treated PTCDI film can be ascribed to H-aggregates.

Optical absorption spectrum of PDPA thin film (Fig. 2a, curve 3) shows a broad absorption band with maximum at 424 nm and a shoulder at 378 nm corresponding to S_0–S_1 transitions in the conjugated polymer chains. Spectrum of the untreated (as prepared) PDPA/PTCDI composite film containing 22 wt% of PTCDI (Fig. 2a, curve 4) can be characterized as a simple superposition of absorption bands of the parent-compounds, the PTCDI bands being broadened owing to the solid-state environment. This observation clearly indicates that PTCDI is molecularly dispersed in the PDPA matrix. This layer served as a base layer for the type II devices.

Changes taking place in the course of the solvent-vapor treatment in double layer systems based on a spin-cast PDPA layer with vacuum deposited thin film of PTCDI (type I device) are shown in Figs. 2–4. Such double layer system does not show marked changes in the optical absorption spectra upon toluene vapor treatment (compare curve 1 and curve 2 in Fig. 2b) except for an increased extinction at short wavelength region. However, the AFM images and corresponding profiles (Figs. 3a, b and 4a) clearly show a growth of PTCDI crystals. The increased extinction at shorter wavelengths can be ascribed to the more pronounced light scattering on bigger crystals grown during the treatment. The peak roughness of untreated system does not exceed several nanometers, which corresponds to the observations of other authors that films of PTCDI derivatives prepared by chemical vapor deposition on an amorphous substrate are amorphous or polycrystalline [35,37]. Degree of crystalinity of such films depends on the deposition conditions and on the structure of substituents [36,38]. In the present case, the deposition was carried out slowly (deposition rate 0.1 nm/s) resulting in polycrystalline structure of the PTCDI layer.

The systems of type II, PDPA + PTCDI/PTCDI, undergo more pronounced evolution upon toluene vapor treatment. The spectrum taken before the vapor treatment shown in Fig. 2c, curve 1 displays contributions of PDPA, molecularly dissolved PTCDI and crystalline PTCDI (shoulder at 590 nm). It corresponds to the superposition of the bottom layer composed of PTCDI molecularly dissolved in PDPA (curve 4 in Fig. 2a) and the upper PTCDI crystalline layer. After only 2 min treatment in toluene vapors, crystallization of PTCDI inside the bottom layer occurs as evidenced by the decrease in peaks at 525 and 489 nm attributed to the molecularly dissolved fraction of PTCDI and simultaneous increase in the peak at 594 nm (curve 2 in Fig. 2c). After 15 min of treatment, the peaks at 525 nm and 489 nm disappear and all PTCDI is in its crystalline form (curve 3). The progressive growth of crystals, which can be followed by AFM (Fig. 3c and d), causes changes in the peak roughness (defined as the height of the highest peak in the roughness profile over the evaluation length) from several nm to ca. 150 nm (Fig. 4b, curve 4).

The morphological changes in the PTCDI layer can be explained by a solvent uptake by the PDPA polymer due to its swelling capability given by exceptionally high gas permeability and fractional free volume together with its good solubility [39]. This unusual property of the PDPA stems from the rigidity of the polymer main chain together with the presence of voluminous trimethylsilyl side-groups. In our experiment with crystal balance monitor we found that 100 nm thick polymer layer can accept as much as 50 wt% of toluene. After 18 h of toluene vapor treatment, large elongated crystals of PTCDI are formed on the polymer surface, with length exceeding 2 μm (Fig. 3f). On the other hand, only small changes in morphology of PTCDI layer of similar thickness deposited on a glass substrate were observed after 18 h treatment.

The crystallization can be further influenced by the presence of molecularly dispersed PTCDI in the bottom polymer layer (compare Fig. 3b and d). Our previous experiments have shown that 15 min of toluene vapor treatment of 120 nm thick PDPA layer containing

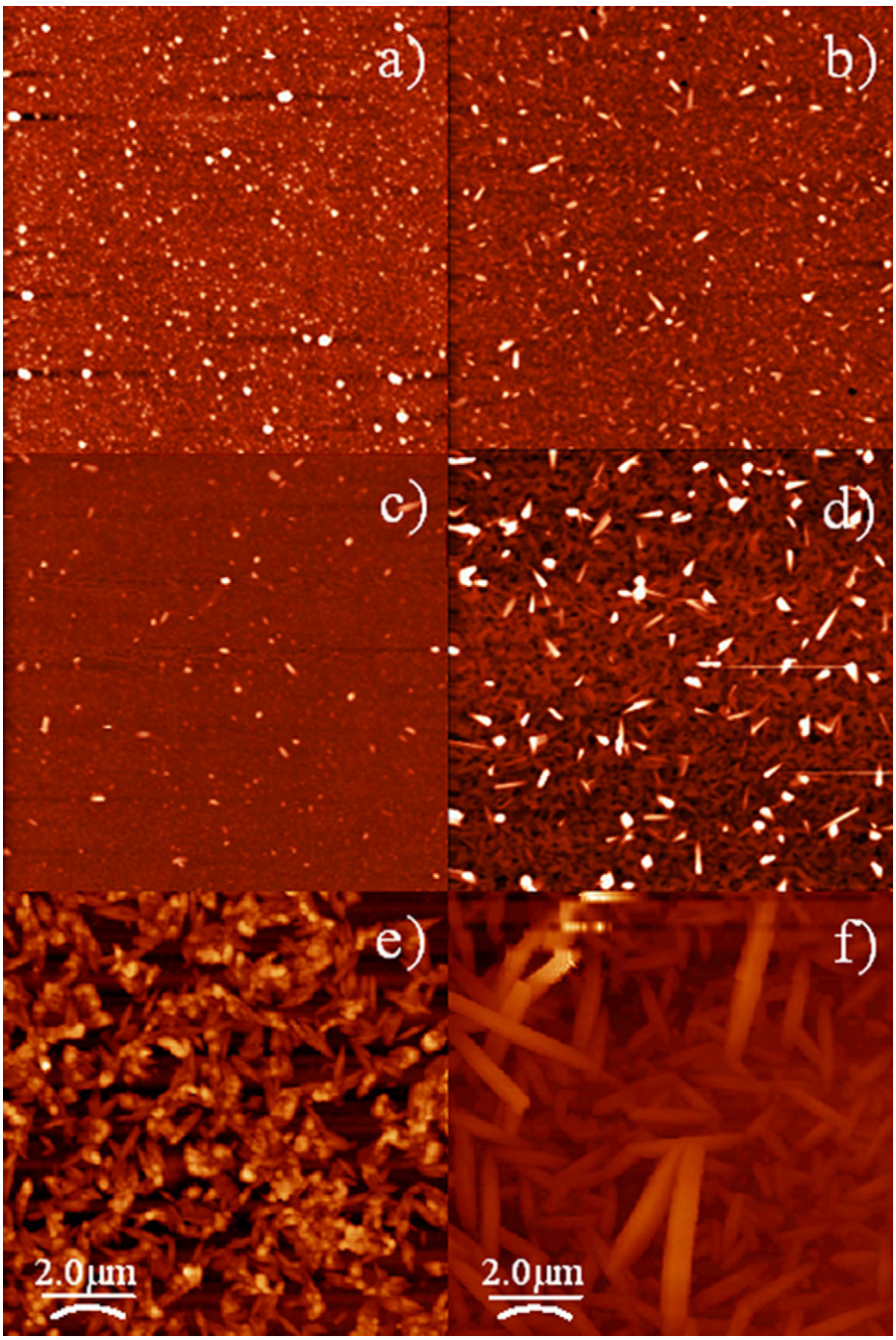

Fig. 3. AFM images on fused silica substrates of (a) system I as prepared, (b) system I after 15 min exposition to solvent vapor, (c) system II as prepared, (d) system II after 15 min treatment, (e) mixed layer PTCDI/PDPA (31 wt% of PDPA, layer thickness 120 nm), (f) double layer PDPA (120 nm)/PTCDI (50 nm) after 18 h of solvent vapor treatment.

31 wt% of molecularly dispersed PTCDI leads to a formation of irregular crystals with the size in 150 nm scale (Fig. 3e). When the mixed layer is combined with deposited top layer of PTCDI the perylene molecules yield, similarly to system I, the elongated shape crystals but their formation is faster.

The energy diagram for our devices is shown in Fig. 5; HOMO–LUMO energy levels of PDPA were obtained from cyclic voltammetry and UV/vis spectroscopy measurements, values for PTCDI in both in crystalline and amorphous form were taken from the literature [27,29]. As can be seen from mutual positions of HOMO and LUMO energy levels, a photoexcitation of both materials forming the heterojunction can lead to the formation of free charge carriers: upon photoexcitation of PDPA, the electron transfer from the PDPA LUMO level to the LUMO level of PTCDI is feasible and, vice versa, upon photoexcitation of PTCDI, the electron transfer from the PDPA HOMO level to the vacant HOMO level of PTCDI is possible, too. Both kinds of electron transitions result in a formation of free electron–hole pairs in the system. ITO layer, being the illuminated electrode, acquires a positive charge in all systems under study.

The spectra of short circuit photocurrent, I_{sc}, expressed as IPCE (incident photon-to-electron conversion efficiency) for devices of type I in various treatment times are given in Fig. 6. The IPCE spectrum of the untreated sample of system I shows the contribution from the polymer (424 and 378 nm) and both crystalline (shoulder at 570 nm) and amorphous phase (525 and 490 nm) of the top PTCDI

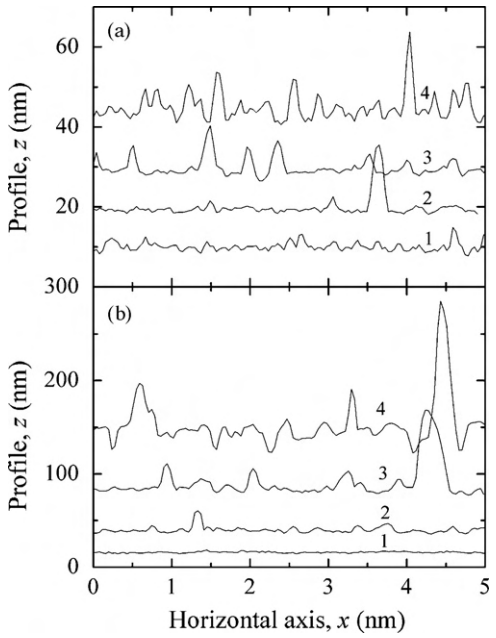

Fig. 4. Profiles derived from the AFM images—(a) system I: curve (1) untreated, (2) after 2 min treatment, (3) after 5 min, and (4) after 15 min treatment with toluene vapor; (b) system II: curve (1) untreated, (2) after 2 min treatment, (3) after 5 min, and (4) after 15 min treatment with toluene vapor.

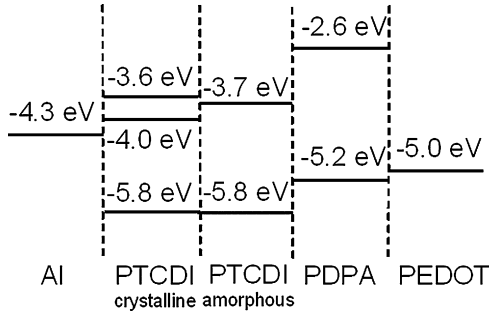

Fig. 5. HOMO and LUMO levels of active components with respect to the work functions of electrodes.

layer. This mixed spectrum is surprising because it follows from the absorption spectra that the top layer is composed mostly from the crystalline phase. After the insertion of the sample in the toluene vapors, the IPCE spectrum in the green-red region is changed and corresponds to the fully crystalline PTCDI layer. Simultaneously, a marked increase in IPCE efficiency was observed for short treatment times 2 and 5 min. At longer treatment times (shown for 15 min treatment in Fig. 6a) a decrease in efficiency was observed, nevertheless the IPCE spectrum maintains the crystalline phase features.

The effect of vapor treatment on the volt–ampere (*V–A*) characteristics of the system I is shown in Fig. 7a. The power conversion efficiency values as determined from *V–A* characteristics (Table 1)

Table 1
Power conversion efficiencies, η [%], of photovoltaic devices based on PDPA and PTCDI obtained at various treatment times

	0 min	2 min	5 min	15 min
I	0.008	0.026	0.022	0.010
II	0.053	0.038	0.036	0.011

Illumination: 10 mW cm^{-2}.

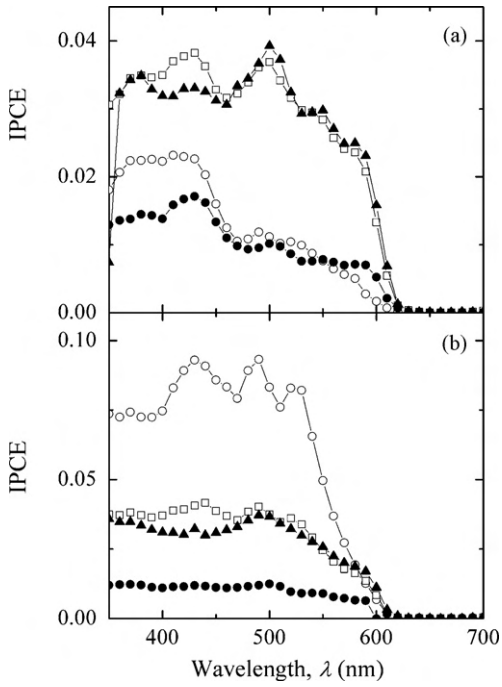

Fig. 6. Incident photon-to-electron conversion efficiency (IPCE) of (a) system I and (b) system II. Open circles: untreated sample, squares: 2 min treatment, triangles: 5 min treatment, full circles: 15 min treatment with toluene vapor.

show an increase of η_e at intermediate treatment times between 2 and 5 min. Because the AFM and optical absorption measurements proved the growth of PTCDI crystals on account of a decrease of amorphous PTCDI and recrystallization of small crystals into the larger ones, the increase in η_e can be explained mainly by more effective electron transport in larger PTCDI crystals resulting in an improved collection efficiency of the photogenerated electrons. It is known from the literature that PTCDI is very good electron-

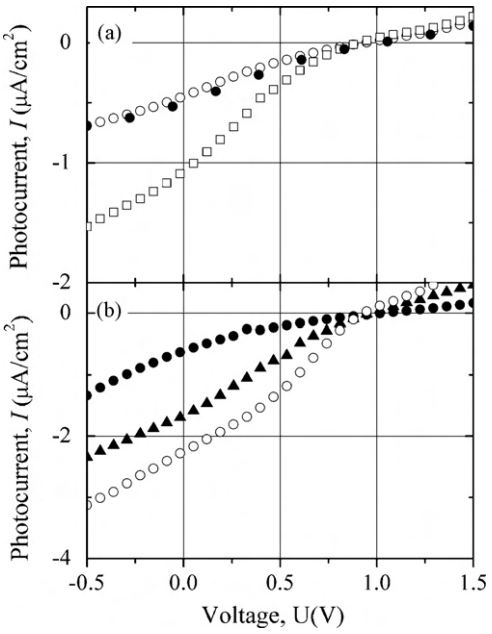

Fig. 7. Photocurrent–voltage characteristics of prepared PV devices under white light illumination (10 mW/cm^2) for (a) system I and (b) system II. Open circles: untreated sample, squares: 2 min treatment, triangles: 5 min treatment, full circles: 15 min treatment with toluene vapor.

transporting material with charge carrier mobility approaching $0.2\,cm^2\,V^{-1}\,s^{-1}$ [40]. This value was obtained from the transient microwave measurement that reflects the short-range mobility inside the crystal domains. On the other hand it is known from the time-of-flight measurements that the long-range electron transport is affected by deep trapping and/or recombination at the grain boundaries [41]. Hence, we can expect that an increase in the size of crystal domains would lead to an improved electron transport. Besides that, the photogeneration in J-aggregates should extend the IPCE spectrum to the red region and so further contribute to the increased overall power conversion efficiency, η (Fig. 6a). As can be seen, a longer-time (15 min) vapor treatment of a sample I turns the efficiency back to almost original value found before the treatment. It can be explained by increased roughness of the PTCDI upper layer, which lowers the interphase area for the charge carrier photogeneration. As a result, a decrease in η is observed though the electron transport is improved in this system.

The system II was designed and prepared in such a way that it contained the same total amount of PTCDI in the whole double layer structure as the system I, which means that the upper layer of system II was thinner on expense of PTCDI molecularly dispersed in the bottom layer. The total thickness (108 nm) was the same for both systems. The redistribution of PTCDI substantially changed the photoelectrical behavior of the system II compared to that the system I. Values of η for untreated (as prepared) samples of type II are several times higher than those observed for the untreated system I. Moreover, the photocurrent spectrum of sample II clearly shows spectral features of molecularly dispersed PTCDI. Unlike the case of system I, the toluene-vapor treatment decreases the overall efficiency of the system II. The IPCE spectra progressively change within first 5 min of the treatment: the spectrum acquires the features typical of crystalline PTCDI and becomes similar to that of the system I treated for the same period of time. During further treatment the system II behaves similarly to the system I. The power conversion efficiencies (Table 1) obtained from *V–A* characteristics (Fig. 7) confirm the high efficiency derived from IPCE spectra and follow the decreasing trend during the vapor treatment.

In our previous experiments [34] we investigated devices based on PDPA/PTCDI mixture containing 31 wt% of PTCDI molecularly dissolved in the polymer matrix. The device that was not subjected to the solvent treatment showed very low PV energy conversion efficiency (3×10^{-5}%) despite its good charge carrier photogeneration ability. The IPCE values measured 2 s after the beginning of the illumination reached 6%, but the IPCE decreased about one order of magnitude during further illumination within the time range of several tens of seconds. This relaxation of the photocurrent negatively influencing the PV efficiency was explained by the development of the space charge due to the insufficient drain of photogenerated free electrons from a site of photogeneration owing to the absence of percolation in that system. Taking those results into account we cannot explain the here-observed increased conversion efficiency in system II by a simple superposition of the effects of bulk and bilayer heterojunction in one device. Obviously, the higher IPCE values could be partially explained by a higher optical extinction of isolated molecules compared to the aggregates and, hence, by a higher amount of absorbed photons. Nevertheless, when recalculating the incident photon-to-electron conversion efficiency per absorbed photons, we still obtain higher values for system II than expected from a simple superposition of effects.

One possible explanation of the observed increase in IPCE of untreated system II that should be discussed is the fact that a thinner upper layer of PTCDI (18 nm vs. 38 nm in system II and I, respectively) can allow for a better collection of charges photogenerated in the crystalline top PTCDI layer in the vicinity of the interface with the bottom polymer layer. But there are some bottlenecks of such explanation: (i) the feature of IPCE spectrum shows that the charges are preferably generated in the bottom polymer phase with molecularly dispersed PTCDI and (ii) if the transport of charges is somehow limited by a polycrystalline structure of the top layer it should be improved upon short toluene-vapor treatment due to recrystallization and not decreased as it was observed in our experiment.

It seems to be clear that molecularly dispersed PTCDI molecules contribute to the overall power conversion efficiency. The only explanation could be the synergy effect of dispersed PTCDI molecules in the bottom layer with the PTCDI in a crystalline form deposited on the top. On the basis of these considerations, the whole PV process in the device II that was not subjected to solvent treatment can be described as follows. The energy absorption occurring in both PDPA and PTCDI is followed by generation of the charges that is efficient mainly at the PDPA/molecularly dissolved PTCDI interface. The holes are transported by PDPA and collected on ITO electrode, the PTCDI facilitates the electron collection by the opposite Al electrode. More detailed mechanism cannot be proposed yet. A decrease in the PV efficiency of the system II upon longer-time solvent treatment probably results from a decrease in (i) the content of molecularly dissolved PTCDI and (ii) in the contact area between the phases similarly as in the device I.

Considering the absolute value of PV efficiency of the as prepared system II under illumination of $10\,mW\,cm^{-2}$, $\eta = 0.05\%$ and the fill factor, FF = 0.3 we obtain values similar to those reported for devices based on poly(3-hexylthiophene)/perylene derivative, but lower than the best reported one with $\eta = 0.18\%$ shown in [27]. In these devices, the PTCDI occurs exclusively in the crystals with dimensions of hundreds of nanometers due to its relatively high concentration. All systems under investigation have similar U_{oc} about 0.95 V which is relatively high, compared to similar devices based on poly(3-hexylthiophene)/perylene derivative giving typically U_{oc} of 0.3 V [29] or a substituted hexabenzocoronene/PTCDI with 0.7 V [28]. If we consider that U_{oc} is given by the difference as a difference between HOMO level of the polymer and LUMO level of J-aggregates of PTCDI (lowest energy level for electron transport) we obtain U_{oc} value to be 1.2 V, slightly higher than the result obtained in our experiments. The fill factor of our best device FF = 0.3 is reasonable compared to devices using perylene based acceptors [28,29] despite a high serial resistance seen from the tangent of current vs. voltage curve at $I = 0$ A.

4. Conclusions

The polymer PDPA showed strong ability to facilitate crystallization of planar perylene type molecules. In the studied double-layer system the PTCDI molecules crystallized into long hair-like crystals that are favorable for electron transport. Nevertheless the obtained results point to the existence of application limits of the solvent-vapor-treatment method in tuning the performance of a bilayer PV device composed of a hole-conducting conjugated polymer such as PDPA and electron-conducting low-molecular-weight compound such as perylene derivative PTCDI. In particular, a solvent-vapor-induced increase in a continuity of the acceptor phase, which improves the collection efficiency of electrons, is achieved on account of a decrease in the PDPA–PTCDI interphase area, which inevitably lowers the efficiency of charge carriers photogeneration. As a result, a maximum occurs on the dependence of PV efficiency of the bilayer device on the time of solvent-vapor treatment.

Compared to the solvent-vapor-treatment method, significantly higher increase in the PV efficiency can be achieved via a construction of a device in which both bulk and bilayer heterojunctions are

present. This can be easily achieved using a polymer phase containing molecularly dissolved PTCDI in the construction of bilayer device. Such device shows better PV efficiency due to the effective combination of free charge carrier photogeneration and its collection and transport to electrodes.

Acknowledgements

The financial support of the Czech Science Foundation (203/06/P226), of Ministry of Education of the Czech Republic (MSM 0021620857) and Grant Agency of the Academy of Sciences of the Czech Republic (A4050406) are greatly acknowledged. The authors would like to thank Dr. M. Špírková for her helpful advice in AFM imaging.

References

[1] C.W. Tang, Appl. Phys. Lett. 48 (1986) 183.
[2] J. Rostalski, D. Meissner, Sol. Energy Mater. Sol. Cells 63 (2000) 37.
[3] P. Peumanns, S.R. Forrest, Appl. Phys. Lett. 79 (2001) 126.
[4] M. Hiramoto, H. Fujiwara, M. Yokoyama, Appl. Phys. Lett. 58 (1991) 1062.
[5] G. Yu, A.J. Heeger, J. Appl. Phys. 78 (1995) 4510.
[6] G. Yu, J. Gao, J.C. Hummelen, F. Wudl, A.J. Heeger, Science 270 (1995) 1789.
[7] H. Hoppe, T. Glatzel, M. Niggemann, W. Schwinger, F. Schaeffler, A. Hinsch, M.C. Lux-Steiner, N.S. Sariciftci, Thin Solid Films 511 (2006) 587.
[8] H. Hoppe, M. Niggemann, C. Winder, J. Kraut, R. Hiesgen, A. Hinsch, D. Meissner, N.S. Sariciftci, Adv. Funct. Mater. 14 (10) (2004) 1005.
[9] M. Reyes-Reyes, K. Kim, D.L. Carroll, Appl. Phys. Lett. 87(8) (2005) 083506.
[10] W.L. Ma, C.Y. Yang, X. Gong, K. Lee, A.J. Heeger, Adv. Funct. Mater. 15 (10) (2005) 1617.
[11] F. Padinger, R.S. Rittberger, N.S. Sariciftci, Adv. Funct. Mater. 13 (2003) 85.
[12] D. Chirvase, J. Parisi, J.C. Hummelen, V. Dyakonov, Nanotechnology 15 (2004) 1317.
[13] L. Chen, D. Godovsky, O. Inganas, J.C. Hummelen, R.A.J. Janssen, M. Svensson, M.R. Andersson, Adv. Mater. 12 (2000) 1367.
[14] M. Drees, K. Premarante, W. Graupner, J.R. Heflin, R.M. Davis, D. Marciu, M. Miller, Appl. Phys. Lett. 81 (2002) 1.
[15] M. Pavlik, J. Pfleger, C. Jossifov, J. Vohlidal, Macromol. Symp. 212 (2004) 555.
[16] J. Pfleger, M. Pavlik, J. Vohlidal, React. Funct. Polym. 65 (2005) 79.
[17] J. Vohlidal, J. Sedlacek, N. Patev, O. Lavastre, P.H. Dixneuf, S. Cabioch, H. Balcar, J. Pfleger, V. Blechta, Macromolecules 32 (1999) 6439.
[18] J. Vohlidal, Z. Kabatek, M. Pacovska, J. Sedlacek, Z. Grubisic-Gallot, Collect. Czech. Chem. Commun. 61 (1996) 120.
[19] J. Sedlacek, J. Vohlidal, Collect. Czech. Chem. Commun. 68 (2003) 1745.
[20] V. Percec, J.G. Rudick, Macromolecules 38 (2005) 7241.
[21] A.S.M. Karim, A.R. Nomura, T. Masuda, J. Polym. Sci. Polym. Chem. 39 (2001) 3130.
[22] K. Tsuchihara, T. Masuda, T. Higashimura, Macromolecules 25 (1992) 5816.
[23] K. Tsuchihara, T. Masuda, T. Higashimura, J. Polym. Sci. A Polym. Chem. 31 (1993) 547.
[24] T. Masuda, J. Polym. Sci. Polym. Chem. 45 (2007) 165.
[25] T. Sakaguchi, K. Yumoto, Y. Shida, M. Shiotsuki, F. Sanda, T. Masuda, J. Polym. Sci. Polym. Chem. 44 (2006) 5028.
[26] J.J. Dittmer, E.A. Marseglia, R.H. Friend, Adv. Mater. 12 (2000) 1270.
[27] J. Li, F. Dierschke, J. Wu, A.C. Grimsdale, K. Muellen, J. Mater. Chem. 16 (2006) 96.
[28] L. Schmidt-Mende, A. Fechtenkotter, K. Muellen, E. Moons, R.H. Friend, J.D. MacKenzie, Science 293 (2001) 1119.
[29] W.S. Shin, H.H. Jeong, M.K. Kim, S.H. Jin, M.R. Kim, J.K. Lee, J.W. Lee, Y.S. Gal, J. Mater. Chem. 16 (2006) 384.
[30] A.J. Makinen, A.R. Melnyk, S. Schoemann, R.L. Headrick, Y.L. Gao, Phys. Rev. B 60 (1999) 14683.
[31] B.A. Gregg, J. Sprague, M.W. Peterson, J. Phys. Chem. B 101 (1997) 5362.
[32] W.B. Genetti, R.J. Lamirand, B.P. Grady, J. Appl. Polym. Sci. 70 (9) (1998) 1785.
[33] J.K. Jeszka, A. Tracz, A. Sroczynska, J. Ulanski, H. Muller, T. Pakula, M. Kryszewski, Synth. Met. 103 (1–3) (1999) 1820.
[34] K. Podhajecka, J. Pfleger, Eur. Phys. J. Appl. Phys. 36 (2006) 241.
[35] J. Mizugichi, Dyes Pigments 70 (2006) 226.
[36] P. Schouwink, G. Gardet, R.F. Mahrt, Chem. Phys. Lett. 341 (2001) 213.
[37] E. Lifshitz, A. Kaplan, E. Ehrenfreund, D. Meissner, J. Phys. Chem. B 102 (1998) 967.
[38] P. Schouwink, A.H. Schafer, C. Seidel, H. Fuchs, Thin Solid Films 372 (2000) 163.
[39] L.G. Toy, K. Nagai, B.D. Freeman, I. Pinnau, Z. He, T. Masuda, M. Teraguchi, Y.P. Yampolskii, Macromolecules 33 (2000) 2516.
[40] C.W. Struijk, A.B. Sieval, J.E.J. Dakhorst, M. van Dijk, P. Kimkes, R.B.M. Koehorst, H. Donker, T. Schaafsma, S.J. Picken, A.M. van de Craats, J.M. Warman, H. Zuilhof, E.J.R. Sudholter, J. Am. Chem. Soc. 122 (2000) 11057.
[41] A. Rybak, J. Pfleger, J. Jung, M. Pavlik, I. Glowacki, J. Ulanski, K. Mullen, Y. Geerts, Synth. Met. 156 (2006) 302.